Structure, Vol. 13, 1809–1817, December, 2005, ©2005 Elsevier Ltd All rights reserved. DOI 10.1016/j.str.2005.08.012

Structure and Mechanism of Imidazoleglycerol-Phosphate Dehydratase

Steven E. Glynn,[1] Patrick J. Baker,[1] Svetlana E. Sedelnikova,[1] Claire L. Davies,[1] Thomas C. Eadsforth,[1] Colin W. Levy,[1,4] H. Fiona Rodgers,[1] G. Michael Blackburn,[2] Timothy R. Hawkes,[3] Russell Viner,[3] and David W. Rice[1,*]

[1] Krebs Institute for Biomolecular Research
Department of Molecular Biology and Biotechnology
University of Sheffield
Firth Court
Western Bank
Sheffield, S10 2TN
United Kingdom

[2] Krebs Institute for Biomolecular Research
Department of Chemistry
University of Sheffield
Sheffield, S3 7HF
United Kingdom

[3] Syngenta
Jealott's Hill International Research Station
Bracknell
Berks, RG42 6EY
United Kingdom

Summary

The structure of *A. thaliana* imidazoleglycerol-phosphate dehydratase, an enzyme of histidine biosynthesis and a target for the triazole phosphonate herbicides, has been determined to 3.0 Å resolution. The structure is composed of 24 identical subunits arranged in 432 symmetry and shows how the formation of a novel dimanganese cluster is crucial to the assembly of the active 24-mer from an inactive trimeric precursor and to the formation of the active site of the enzyme. Molecular modeling suggests that the substrate is bound to the manganese cluster as an imidazolate moiety that subsequently collapses to yield a diazafulvene intermediate. The mode of imidazolate recognition exploits pseudosymmetry at the active site arising from a combination of the assembly of the particle and the pseudosymmetry present in each subunit as a result of gene duplication. This provides an intriguing example of the role of evolution in the design of Nature's catalysts.

Introduction

The market for herbicides that are applied after the emergence of the crop is currently dominated by compounds that act at a limited number of biological targets, each of which now faces increasing challenges with respect to the emergence of herbicide-resistant weeds (Guttieri et al., 1992; Devine, 1997; Preston and Powles, 2002). Given the paucity of biological targets, there is an urgent need for the development of new herbicides with novel modes of action.

Histidine is an essential dietary nutrient for animals, but it is synthesized de novo by plants and microorganisms. Thus, the pathway of histidine biosynthesis is a potential target for herbicide development. Imidazoleglycerol-phosphate dehydratase (IGPD; EC 4.2.1.19) catalyzes the sixth step in the histidine biosynthesis pathway, the dehydration of imidazoleglycerol-phosphate (IGP) to form imidazoleacetol-phosphate (IAP). While the mechanism of the enzyme is currently unknown, the identification of a novel class of phloem mobile herbicides, the triazole-phosphonates, as potent inhibitors of IGPD has suggested that the reaction may proceed through a diazafulvene intermediate (Gohda et al., 1998; Hawkes et al., 1993).

Previous studies on the characterization of IGPD from a number of different species have shown that, in the presence of EDTA, the apo-protein exists as a catalytically inactive trimer, but upon addition of Mn^{2+} or a number of divalent cations (e.g., Co^{2+}, Cd^{2+}, Ni^{2+}, Fe^{2+}, and Zn^{2+}), this trimeric precursor assembles to form a biologically active 24-mer containing ~1.5 metal ions/monomer (Petersen et al., 1997; Tada et al., 1995) and exhibiting 432 symmetry (Hawkes et al., 1995; Wilkinson et al., 1995). One ion, oxovanadium, assembles the enzyme correctly, but in a catalytically inactive form, suggesting that metal ions are critical not only to subunit assembly, but also in playing a fundamental role in catalysis (Petersen et al., 1997). Recently, the structure of the trimeric form of IGPD from the fungus *Filobasidiella neoformans* has been determined (Sinha et al., 2004) to reveal that each subunit can be divided into two half-monomers that are related by 2-fold pseudosymmetry and whose sequences are indicative of an ancient gene duplication event that led to the formation of the current enzyme. However, the absence of bound metals in this structure, the presence of disorder in one of the two histidine-rich motifs that have been proposed to be involved in metal binding and catalysis, and the lack of information on the precise mode of subunit assembly prevented a detailed examination of the molecular basis of specificity and catalysis.

In this paper, we report the structure of the manganese assembled, active form of *Arabidopsis thaliana* IGPD at 3.0 Å resolution. Analysis of the structure has revealed a novel, to our knowledge, manganese cluster that is critical in converting the inactive trimeric state of the enzyme into its biologically active 24-mer and that also forms the active site. Preliminary modeling studies on the mode of binding of a diazafulvene intermediate have permitted the identification of key residues that are important in substrate recognition and catalysis and have opened up the possibility of developing a program of rational herbicide design. Furthermore, the structure has shown how the gene duplication seen in IGPD has played a key role in the evolution of the catalytic properties of the enzyme.

*Correspondence: d.rice@sheffield.ac.uk
[4] Present address: Faculty of Life Sciences, Jackson's Mill, The University of Manchester, P.O. Box 88, Sackville Street, Manchester, M60 1QD, United Kingdom.

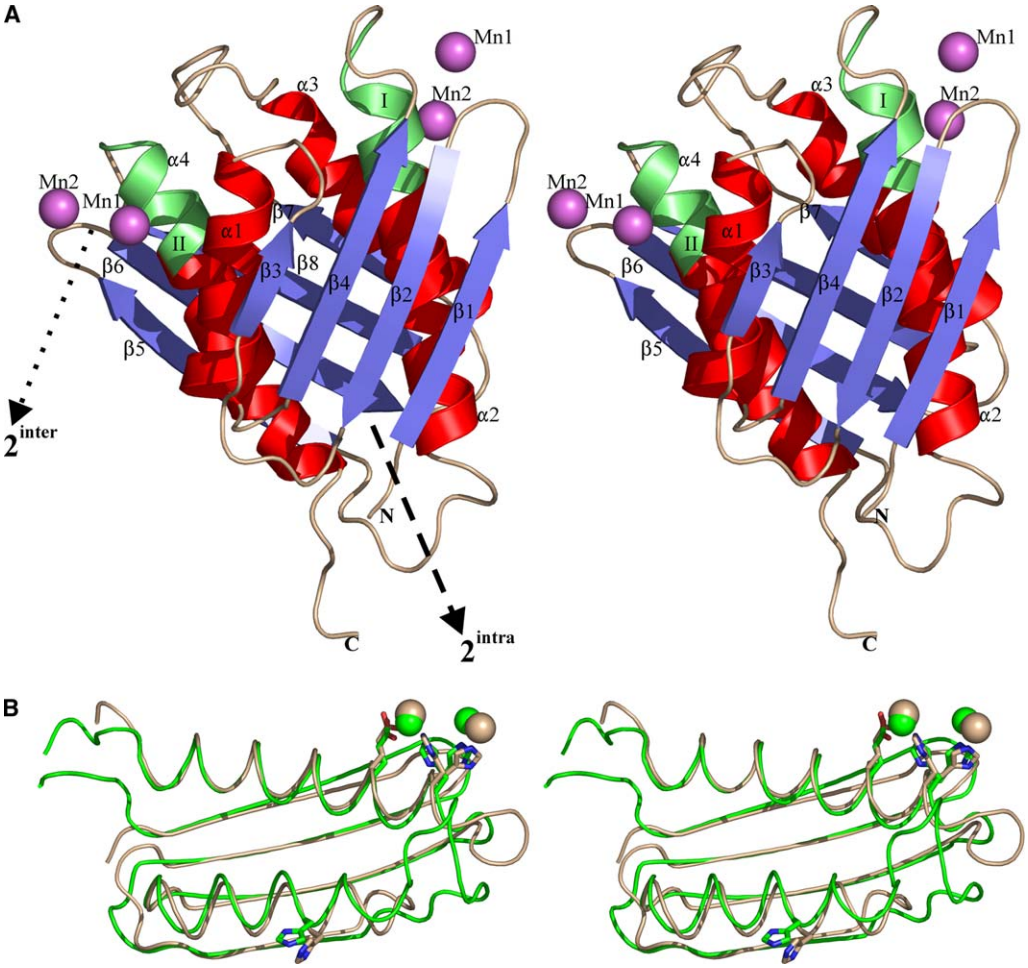

Figure 1. The Structure and Pseudosymmetry of the IGPD Monomer

(A) Stereodiagram showing the structure of the *A. thaliana* IGPD monomer. The four "half"manganese ions associated with each subunit are shown as purple spheres. The two histidine-rich motifs present within the monomer (motifs I and II) are colored green and labeled. The approximate positions of the intra- and intersubunit 2-fold pseudosymmetry axes are shown as a dashed arrow and a dotted arrow, respectively, and are labeled.

(B) Stereodiagram showing the pseudosymmetry within the IGPD monomer. Residues 10–94 (beige) are superimposed onto residues 95–192 (green). Residues that coordinate the manganese ions are shown in ball-and-stick format, with the four manganese ions colored according to whether they are associated with the N- or C-terminal halves of the molecule.

Results and Discussion

Structure of the *A. thaliana* IGPD Monomer

The structure of the monomer of *A. thaliana* IGPD closely resembles that of the *F. neoformans* enzyme to which it is 49% identical in sequence (rmsd of 1.1 Å over 170 equivalent Cαs of the monomer). The monomer comprises a bundle of four α helices sandwiched between two four-stranded mixed β sheets (Figure 1A) in which the two halves of the molecule can be seen to be related by an axis of 2-fold pseudosymmetry (rmsd of 1.2 Å over 67 Cαs) (Figures 1A and 1B).

Structure of the IGPD 24-Mer

The 24 subunits in *A. thaliana* IGPD are arranged in 432 symmetry to give a particle that has overall dimensions of 110, 120, and 100 Å measured across the 2-, 3-, and 4-fold axes, respectively (Figure 2A). The arrangement of the subunits in this fashion creates a protein "shell," of approximately 35 Å thickness, with a large internal cavity of ~45 Å in diameter (Figure 2B). Small channels lead from the outside to the inside of the 24-mer; the largest of these channels are ~4 Å in diameter across the 4-fold axes and 2 Å across the 3-fold axes. The trimeric arrangement of subunits in the *F. neoformans* enzyme is very closely related to that seen here (rmsd of 1.1 Å over 510 equivalent Cαs), and, qualitatively, the organization of the 24-mer is similar to that favored for the fungal enzyme based on modeling (Sinha et al., 2004).

The Active Site of IGPD

Analysis of the pattern of sequence conservation in the structure of the assembled enzyme reveals that 22 of the 29 conserved residues (Figure 3) cluster between 4-fold-related subunits (Figure 2A) at a region facing the solvent on the exterior surface of the assembled enzyme. This region also exhibits local intersubunit 2-fold pseudosymmetry that is additional to the intrasubunit

2-fold pseudosymmetry and that arises from the combination of the latter with the molecular 4-fold axis to which it is perpendicular (Figure 2C). These conserved residues principally arise from two 4-fold-related subunits (subunits A and A′ of the adjacent trimers ABC and A′B′C′), together with a small number of additional interactions from subunit C (Figure 4). The identification of this region as the active site is also consistent with the observation that a strongly bound sulfate ion can be seen to be surrounded by four basic conserved residues (H55A, R99C, R121C, and K177A). We presume that this represents the site for the phosphate moiety of the substrate. In this way, each IGPD monomer within the assembled enzyme contributes conserved residues to three separate active sites.

Examination of the electron density maps in the active site shows unambiguous density for the presence of two manganese ions per subunit, located 6.65 Å apart and related by the intersubunit pseudo2-fold axis described above. The metal ions are coordinated by residues of two imperfectly repeated histidine-rich sequence motifs with the consensus sequence D/NXHHXXE (motif I, residues 71–77; motif II, residues 167–173, Figure 3) and that have previously been implicated in metal binding (Sinha et al., 2004). However, rather than a single motif binding a single metal ion, the binding of the two manganese ions is a function of four independent "half-sites" involving residues from motif I of one subunit (A′) and residues from motif II of a 4-fold-related subunit (A), each of which contribute to both sites (Figure 2C). Each of the metals is coordinated by two histidines and a glutamic acid arising from these motifs (Mn1: H74A′, H169A, and E173A; Mn2: H73A′, H170A, and E77A′), together with a further conserved histidine (Mn1: H47A; Mn2: H145A′), to form an arrangement of three equatorial and one axial ligands (Figures 2C and 4). We presume that the octahedral coordination of each manganese ion is completed by additional equatorial and axial water molecules that are not visible in the structure at this resolution. Multiple sequence alignments of IGPD from a wide range of species reveal that seven of these eight metal binding residues are completely conserved (Figure 3). In the metal-free *F. neoformans* IGPD model, several residues within motif I are disordered, and their ordering in the *A. thaliana* enzyme appears to be a direct consequence of metal binding. The observation that the active site comprises two metal ions per subunit in similar, but nonidentical, environments is also consistent with spectroscopic data (Petersen et al., 1997, 2000), which suggested the existence of distinct metal subsites, each associated with a multiplicity of coordinating histidyl imidazole ligands.

The Mechanism of IGPD

Currently, the mechanism of the dehydration of IGP to IAP by IGPD is unknown; however, the lack of an adjacent carbonyl or imine group results in a nonacidic leaving proton, in contrast to most dehydration reactions (Gerlt and Gassman, 1992), and suggests an unusual method of catalysis. Experiments with variously deuterated substrates indicate that the reaction is most likely to proceed via a Δ^2-enol (Parker et al., 1995), possibly via a diazafulvene intermediate whose existence is indirectly supported by its similarity, both electronic and steric, to a range of potent triazole-phosphonate IGPD inhibitors (Gohda et al., 1998; Hawkes et al., 1993; Lindell et al., 1996) (Figure 5A). Furthermore, the dependence of IGPD activity on manganese has been shown to be catalytic as well as structural, as IGPD can be assembled by VO^{2+} to yield an inactive enzyme (Petersen et al., 1997). Additionally, it has been suggested that the metal ions facilitate the reaction by forming a coordination complex with the reaction intermediates (Parker et al., 1995), although the exact nature of this is not known.

In our attempt to relate the proposed mechanism of IGPD to the structure, we manually docked the diazafulvene intermediate into the metal-containing cavity of IGPD, superimposing its phosphate onto the sulfate ion observed in the crystal structure and extending the remainder of the molecule along the cavity toward the manganese ions, exploring both the *cis* and *trans* forms of the intermediate about the double bond. The modes of binding of these different isomers is similar in respect to the imidazole and phosphate moieties, but they result in a shift in the positions of the intervening C-1, C-2, and C-3 atoms and the hydroxyl group attached to C-2. Of the alternative isomers, we favored the *cis* form, since it not only offers the opportunity for additional metal chelation to Mn1, but is also consistent with several aspects of the mechanism. In our docked orientation, the phosphate group of the diazafulvene is close to the side chains of three basic residues (Arg99C, Arg121C, and Lys177A), the imidazole ring of His55A, and the side chain amide of Gln51A. The diazafulvene ring makes a nonpolar contact with the side chain of Leu107A and sits between the two manganese ions (Mn1 and Mn2), with the lone pair vectors of each of its two nitrogen atoms coordinating to one of the metal ions. The hydroxyl group of the intermediate is within coordination distance of Mn1, and its proton can be oriented to make a hydrogen bond to the carboxyl oxygen of Glu173A (Figure 4). In this mode of docking, each of the octahedral coordination sites of Mn1 is occupied by either the enzyme or the inhibitor, providing an explanation for both the observed lack of IGPD activity of the oxovanadium (VO^{2+})-assembled enzyme and its relative inability to bind the presumptive diazafulvene-like inhibitors (Petersen et al., 1997). Given the similarity in ionic radius and coordination chemistry, the structure also explains why the Ni^{2+}- and Co^{2+}-assembled enzymes retain significant activity (Petersen et al., 1997).

This docking has enabled us to rationalize some of the mechanistic aspects of the enzyme (Figure 5B). It seems likely that the first step in catalysis is the deprotonation of IGP to form an imidazolate anion. This is presumably favored by the coordination of the imidazole ring to both manganese ions. Once the anion is formed, pi-electron donation from the ring leads to the loss of the C-3 hydroxyl to form the diazafulvene, with the weak (rather than strong) electron withdrawing nature of manganese possibly facilitating this process (Figure 5B, step 1). The bidentate coordination of Mn1 by the imidazolate anion also facilitates the loss of the C-3 hydroxyl stereoelectronically by constraining the (C-3)-OH bond to be roughly orthogonal to the diazafulvene ring, thus maximizing orbital overlap of its pi-electron system with the breaking bond. To generate the Δ^2-enol, removal of

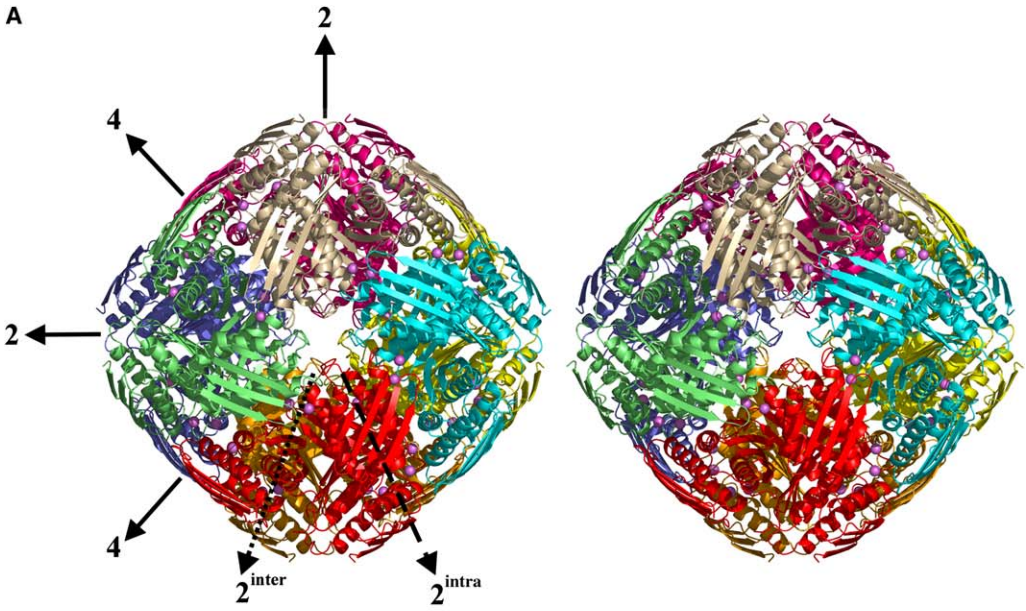
A
2
4
2
4
2inter
2intra

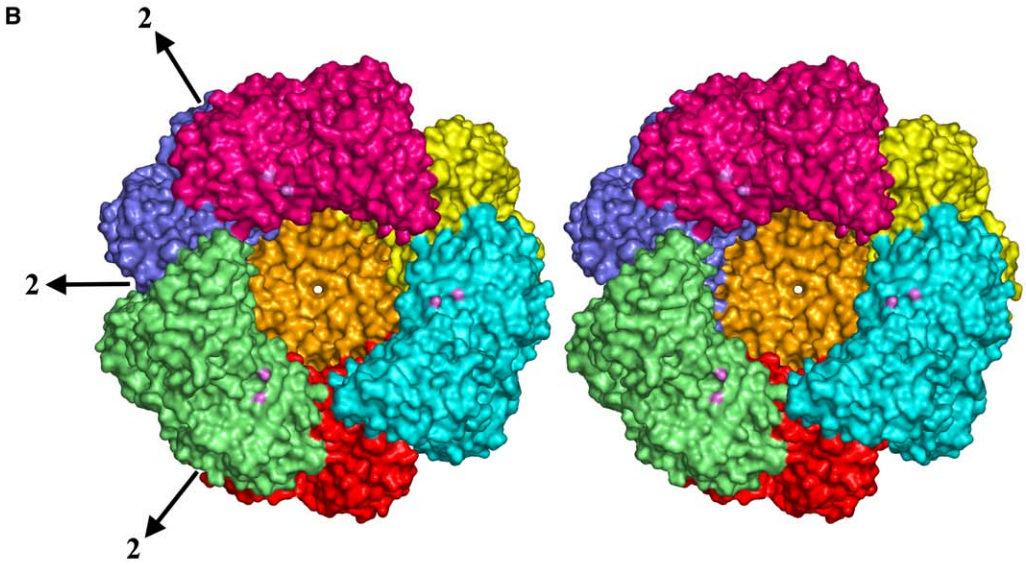
B
2
2
2

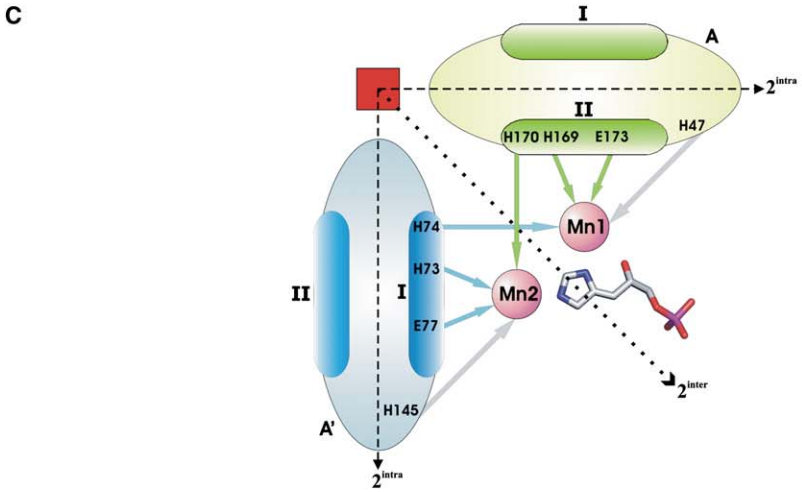
C
I
A
2intra
II
H170 H169 E173
H47
H74
Mn1
H73
Mn2
II
I
E77
2inter
H145
A'
2intra

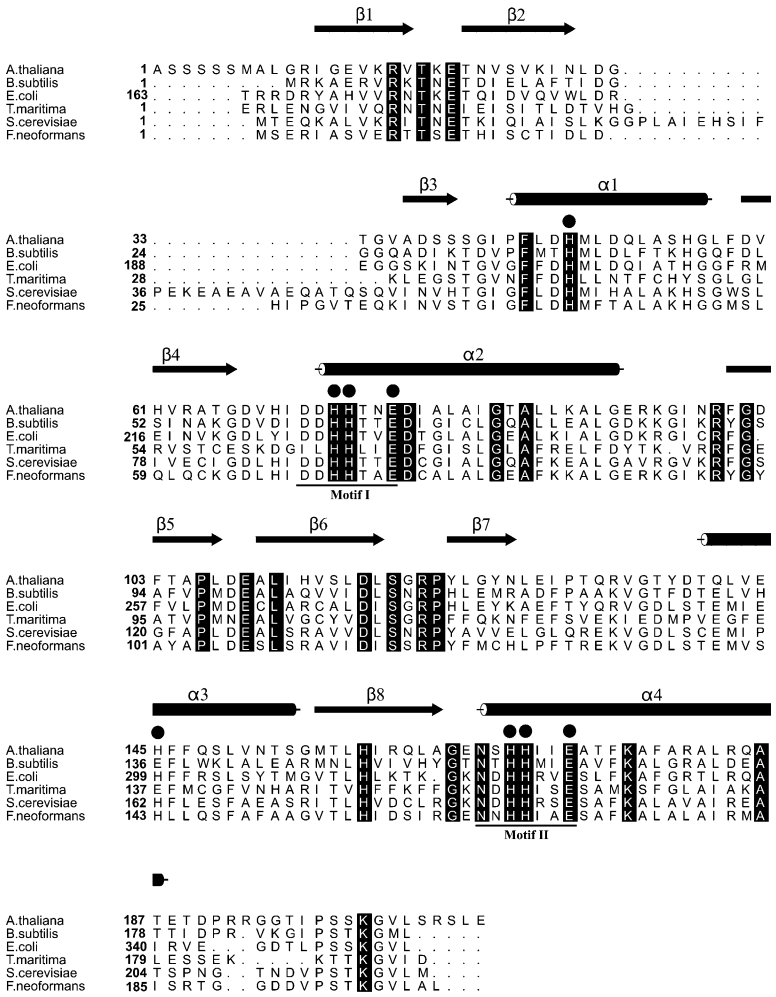

Figure 3. Structure-Based Sequence Alignment Showing the Conservation of Residues across the IGPD Amino Acid Sequences of Six Diverse Species

Residues conserved across all of the species are shown with a black box, and the eight manganese coordinating residues are denoted by a black circle. Helices and strands are shown as cylinders and arrows, respectively, and are labeled. Residue numbers for the start of each line of the corresponding sequence are shown.

the proton on C-2 of the diazafulvene intermediate is required. The coordination of the diazafulvene system to both manganeses can now serve to draw pi-electrons back into the ring and thereby promote the loss of this C-2 proton, possibly involving the carboxyl group of Glu21A′, a fully conserved residue across the IGPD family as a base (Figures 3 and 5B, step 2). Again, the bidentate coordination of Mn1 provides a helpful constraint. This time, the (C-2)-H bond is orthogonal to the diazafulvene system, and the nascent anion can be stabilized by delocalization. While the *trans* conformer of the diazafulvene can be accommodated in the active site without adverse steric interactions, the resulting change in the position of C-2 eliminates the possibility of bidentate coordination of Mn1, suggesting that this mode of binding is less likely.

Since the reaction proceeds with inversion of the stereochemistry at C-3, this suggests that the complete tautomerization is enzyme catalyzed (Whitman et al., 1991; Moore et al., 1993), and, that after abstraction of the C-2 proton, the Δ^2-enol remains bound in much the same way as the diazafulvene intermediate. Examination of the model reveals that Glu173A is well positioned to deprotonate the hydroxyl group of the enol

Figure 2. Symmetry and Pseudosymmetry in the Assembled IGPD 24-Mer

(A) Stereodiagram showing a cartoon representation of the IGPD particle as viewed down the 4-fold axis and colored by trimer, with manganese ions shown as purple spheres. The positions of the 2-fold and 4-fold symmetry axes that lie in the plane of the paper are shown as solid arrows and are labeled by rotational symmetry number. The positions of both the intra- and intersubunit 2-fold pseudosymmetry axes are shown as a dashed arrow and a dotted arrow, respectively, and are labeled.

(B) Stereodiagram showing a surface representation of the IGPD particle as viewed down the 3-fold axis. A total of 21 of the 24 subunits are shown with residues of one trimer missing to show the large internal cavity. The subunits are colored by trimer as in (A), with manganese ions colored purple. The positions of the 2-fold axes that lie in the plane of the paper are shown as solid arrows and are labeled by rotational symmetry number.

(C) A schematic diagram illustrating the role of the manganese ions in promoting assembly around the 4-fold axis. Subunits A and A′ are shown (light green and light blue, respectively) with the two histidine-rich motifs highlighted in corresponding dark colors and are labeled. Residues coordinating the manganese ions are shown as solid arrows and are labeled. The position of the 4-fold axis of the 24-mer is shown as a red square; the intrasubunit 2-fold pseudosymmetry axes shown as dashed arrows bisecting each subunit. The intersubunit 2-fold pseudosymmetry axis created after assembly is shown by a dotted arrow that is straddled by the two manganese ions and the imidazole ring of the diazafulvene intermediate, which are shown as purple spheres and in stick format, respectively.

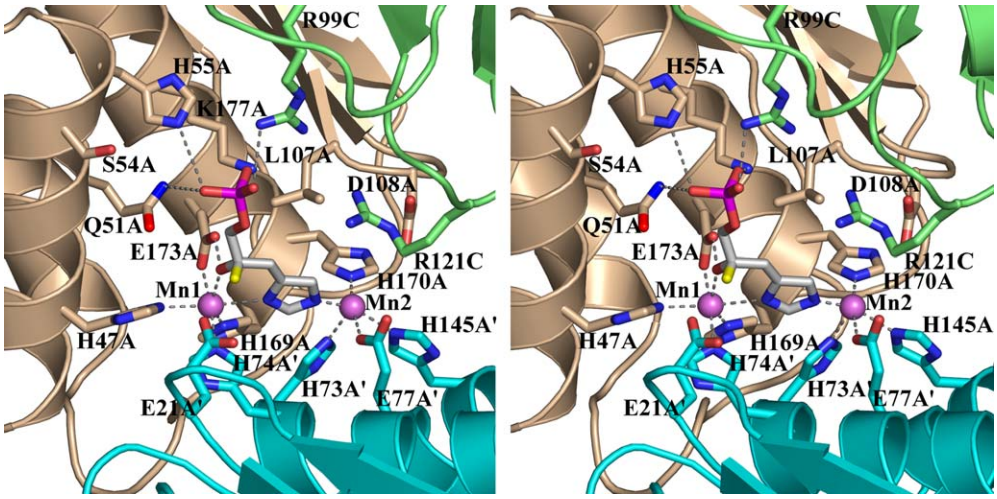

Figure 4. Stereodiagram of the Active Site of *A. thaliana* IGPD

The protein backbone is shown and colored gold, cyan, and green for chains A, A′, and C, respectively. The two manganese ions are shown as labeled purple spheres, and the nonhydrogen atoms of the modeled diazafulvene intermediate are shown in ball-and-stick format and colored by atom, together with the C-2 hydrogen, which is additionally shown and colored yellow. Side chains of residues located within 5 Å of either of the metal ions or of the diazafulvene are shown in ball-and-stick format and labeled; polar interactions are shown as dashed black lines.

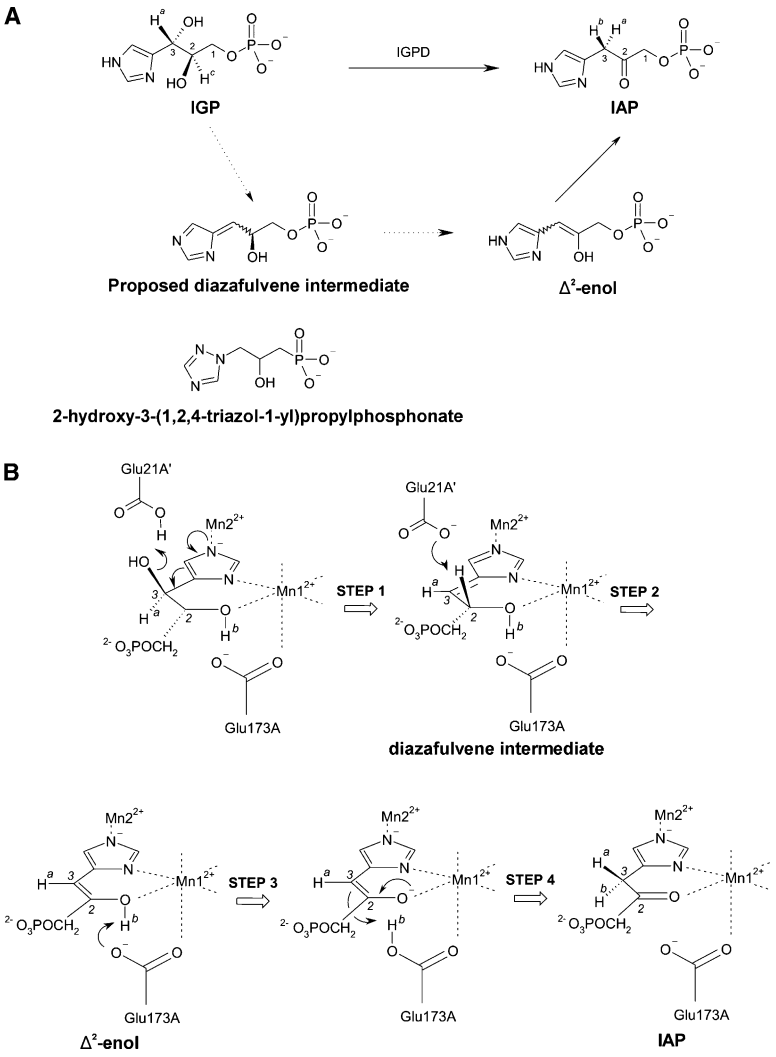

Figure 5. The Proposed Catalytic Mechanism of IGPD

(A) Schematic drawing showing the overall reaction catalyzed by IGPD and the proposed diazafulvene and Δ^2-enol reaction intermediates. The triazole phosphonate inhibitor 2-hydroxy-3-(1,2,4-triazol-1-yl)propylphosphonate is shown to highlight the similarity to the proposed diazafulvene intermediate.

(B) Schematic drawing showing the proposed catalytic mechanism for the conversion of IGP through the diazafulvene and the Δ^2-enol intermediates, to IAP, and detailing how the specific stereochemistry of the reaction may be achieved.

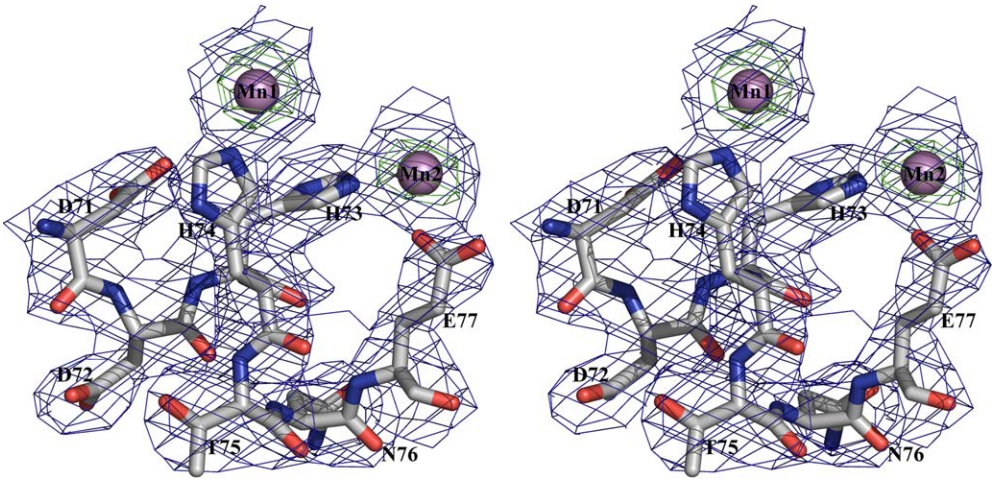

Figure 6. Stereo Representation of the Final $2F_{obs} - F_{calc}$ Electron Density Map Contoured at 1σ around the Histidine-Rich Motif that Is Partly Disordered in the *F. neoformans* Structure

A $F_{obs} - F_{calc}$ electron density difference map is also shown, calculated after initial rigid body refinement of the molecular replacement solution and contoured at 3σ (green). The positions of the two manganese ions, which, along with residues 69–74, were omitted from this model, can be clearly seen. Protein atoms are shown in ball-and-stick format and are colored by atom, and manganese ions are shown as purple spheres.

(Figure 5B, step 3) and relocate this proton to the C-3 carbon in a 1,3-suprafacial proton transfer, thus imposing the net inversion of the configuration at C-3 that is observed (Figure 5B, step 4). The structural similarity between the triazole inhibitor 2-hydroxy-3-(1,2,4-triazol-1-yl)propylphosphonate (Figure 5A), in which the triazole ring mimics the diazafulvene and which would be expected to retain the majority of these interactions, provides powerful supporting evidence for the proposed model.

The Metal Binding Site in IGPD Is Created by Gene Duplication

Comparisons of the structure of IGPD with the structures of proteins that bind two transition metals suggest that the manganese cluster observed here appears to represent a novel arrangement that currently has no counterpart in any structure in the Protein Data Bank (Berman et al., 2000). However, precedence for imidazole rings spanning between two manganese ions can be found in the small-molecule Cambridge Structural Database, which currently has five entries containing this motif with intermanganese distances ranging from 6.25 Å to 6.49 Å (Allen, 2002), corresponding closely to the value observed in IGPD (6.65 Å). This spacing is also similar to that seen in the active site of Cu/Zn superoxide dismutase (SOD), in which a histidine residue bridges the copper and zinc ions to create an imidazolate moiety (Tainer et al., 1982) in a similar manner to that suggested by the modeling of the diazafulvene in IGPD. However, for the two enzymes, both the structures themselves and the symmetry of the metal ligands (octahedral in IGPD versus tetrahedral in SOD) are entirely different, although, in both, a change in the charge status of the imidazole ring during catalysis would appear to be a common feature.

Unlike in Cu/Zn SOD, where the active site is formed from a single monomer, in IGPD, the active site is constructed around the intersubunit 2-fold pseudosymmetry axis whose existence is reliant on both gene duplication and subunit assembly (Figure 2C). This raises a number of intriguing questions about the evolution of the enzyme we see today. Was the ancestor of IGPD formed from a dimer of a subunit of half the size that assembled in 432 symmetry with 48 rather than 24 subunits and that subsequently underwent a later gene duplication event? Alternatively, did the gene duplication create a subunit whose subsequent mutation and assembly gave rise to the enzyme we see today? In this regard, it is interesting to note that the fold of the half-monomer is structurally similar to that of the core of the GHMP kinase superfamily (Sinha et al., 2004). However, there are, to our knowledge, no examples of particles with 48 subunits in this symmetry, and there are no other examples of the pseudosymmetric IGPD fold. This enzyme would therefore seem to provide fascinating insight into the role of evolution in generating Nature's catalysts while simultaneously opening up new opportunities for the development of rationally designed herbicides.

Table 1. Refinement Statistics

Space group	R3
Resolution range (Å)	50.0–3.0
Unit cell parameters (Å)	a = 157.9; b = 157.9; c = 480.0
Number of reflections (working/free)	79,876/4,204
Number of protein non-H atoms	22,176
Manganese atoms	32
Sulfate atoms	80
R factor[a]/R_{free}[b] (%)	24.8/28.6
Rmsd bond lengths (Å)	0.011
Rmsd bond angles (°)	1.35
Ramachandran plot statistics Allowed/disallowed (%)	99.0/1.0

[a] R factor = $\Sigma_{hkl}||F_{obs}| - |F_{calc}||/\Sigma_{hkl}|F_{obs}|$.
[b] R_{free} is the crystallographic R value calculated by using 5% of the data withheld from refinement.

Experimental Procedures

Purification, Crystallization, and Data Collection

A. thaliana IGPD was cloned, expressed, purified, and crystallized as previously described (Glynn et al., 2005). The crystals belong to space group R3 with cell parameters a = 157.9 Å, b = 157.9 Å, c = 480.0 Å, $\alpha = \beta = 90°$, $\gamma = 120°$ and with 16 subunits in the asymmetric unit (Matthews, 1968). Data were collected on a MAR Research image plate by using a Rigaku RU200 rotating anode source to 3.0 Å resolution and were processed with DENZO/SCALEPACK (Otwinowski and Minor, 1997).

Structure Solution

The solution and refinement of the *A. thaliana* IGPD structure were carried out by using the CCP4 suite of programs (CCP4, 1994). Analysis of the self-rotation function calculated with POLARRFN (CCP4, 1994) by using data from 20 to 3 Å resolution and a radius of integration of 15 Å suggested that the cell contained particles in 432 symmetry, with a molecular 3-fold axis of the enzyme aligned parallel to the crystallographic 3-fold axis. The radius of the assembled 24-mer of the *S. cerevisiae* enzyme has been estimated to be ~66 Å (Wilkinson et al., 1995), and, on the basis of this, packing considerations suggest that the cell must contain multiple 24-mers, probably assembled around the independent 3-fold axes present within this space group. The structure was solved by molecular replacement in AMORE (Navaza, 1994), by using the coordinates of the apo *F. neoformans* trimer as a search model. Preliminary analysis of the molecular replacement solutions suggested that they could be combined to produce a convincing model of a 24-mer around the crystallographic 3-fold axis whose center lies at the cell origin and that was formed by the combination of the crystallographic 3-fold symmetry and eight subunits in the asymmetric unit. A molecular replacement search for a second IGPD particle gave a clear solution for an additional 24-mer centered at 1/3, 2/3, 1/6, which is formed around the independent crystallographic 3-fold axis at this position with an additional eight subunits in the asymmetric unit. The presence of additional molecules in the cell is precluded by packing considerations.

Refinement and Analysis

Initial rigid-body refinement of the individual subunits with REFMAC5 (Murshudov et al., 1997) was followed by iterative cycles of rebuilding in TURBO/FRODO (Roussel and Cambillau, 1991) and restrained refinement with tight noncrystallographic (NCS) restraints that were removed toward the end of the refinement. After convergence of the refinement, the resultant electron density map was averaged in DM (Cowtan, 1994) over the 16 copies of the subunit in the asymmetric unit. Examination of the electron density map clearly indicated that the molecular replacement solution was correct through the appearance of unambiguous electron density for residues belonging to the histidine-rich motif (residues 71–77) that was disordered in the *F. neoformans* structure and for two manganese ions associated with each subunit that were not included in the model (Figure 6). The final model has an R factor of 24.8% and an R_{free} of 28.6% and comprises the coordinates of 16 subunits, 32 manganese ions, and 16 sulfate ions (Table 1). In the final model, there is good electron density for the majority of the protein chain, except for residues 1–9, for the C-terminal 17 residues (residues 193–209) that are disordered in all subunits, and the side chains of residues K15, R16, K20, K27, E93, K95, E129, and R192, which have been truncated to Cβ in all subunits. Figures were prepared with PYMOL (Delano) and ALSCRIPT (Barton, 1993).

Acknowledgments

This work was supported by The Biotechnology and Biological Sciences Research Council (BBSRC), The Medical Research Council, and the Wellcome Trust. The Krebs Institute is a designated BBSRC Biomolecular Science Centre and a member of the North of England Structural Biology Centre.

Received: May 27, 2005
Revised: August 18, 2005
Accepted: August 18, 2005
Published: December 13, 2005

References

Allen, F.H. (2002). The Cambridge Structural Database: a quarter of a million crystal structures and rising. Acta Crystallog. B *58*, 380–388.

Barton, G.J. (1993). ALSCRIPT: a tool to format multiple sequence alignments. Protein Eng. *6*, 37–40.

Berman, H.M., Westbrook, J., Feng, Z., Gilliland, G., Bhat, T.N., Weissig, H., Shindyalov, I.N., and Bourne, P.E. (2000). The Protein Data Bank. Nucleic Acids Res. *28*, 235–242.

CCP4 (Collaborative Computational Project, Number 4) (1994). The CCP4 suite: programs for protein crystallography. Acta Crystallog. D Biol. Crystallogr. *50*, 760–763.

Cowtan, K. (1994). DM: an automated procedure for phase improvement by density modification. Joint CCP4 ESF-EACBM Newsletter on Protein Crystallography, *31*, 34–38.

DeLano, W.L. The PYMOL Molecular Graphics System (http://www.pymol.org).

Devine, D.M. (1997). Mechanisms of resistance to acetyl-coenzyme A carboxylase inhibitors: a review. Pestic. Sci. *51*, 259–264.

Gerlt, J.A., and Gassman, P.G. (1992). Understanding enzyme-catalyzed proton abstraction from carbon acids – details of stepwise mechanisms for β-elimination reactions. J. Am. Chem. Soc. *114*, 5928–5934.

Glynn, S.E., Baker, P.J., Sedelnikova, S.E., Levy, C.W., Rodgers, H.F., Blank, J., Hawkes, T.R., and Rice, D.W. (2005). Purification, crystallisation and preliminary crystallographic analysis of *Arabidopsis thaliana* imidazoleglycerol-phosphate dehydratase. Acta Crystallogr. F *61*, 776–778.

Gohda, K., Kimura, Y., Mori, I., Ohta, D., and Kikuchi, T. (1998). Theoretical evidence of the existence of a diazafulvene intermediate in the reaction pathway of imidazoleglycerol phosphate dehydratase: design of a novel and potent heterocycle structure for the inhibitor on the basis of the electronic structure-activity relationship study. Biochim. Biophys. Acta *1385*, 107–114.

Guttieri, M.J., Eberlein, C.V., MallorySmith, C.A., Thill, D.C., and Hoffman, D.L. (1992). DNA-sequence variation in domain A of the acetolactate synthase genes of herbicide-resistant and herbicide susceptible weed biotypes. Weed Sci. *40*, 670–676.

Hawkes, T.R., Cox, J.M., Barnes, N.J., Beautement, K., Edwards, L.S., Kipps, M.R., Langford, M.P., Lewis, T., Ridley, S.M., and Thomas, P.G. (1993). Imidazole glycerol phosphate dehydratase: a herbicide target. Proceedings of the Brighton Crop Protection Conference *6*, 739–744.

Hawkes, T.R., Thomas, P.G., Edwards, L.S., Rayner, S.J., Wilkinson, K.W., and Rice, D.W. (1995). Purification and characterization of the imidazoleglycerol-phosphate dehydratase of *Saccharomyces cerevisiae* from recombinant *Escherichia coli*. Biochem. J. *306*, 385–397.

Lindell, S.D., Earnshaw, C.J., Wright, B.J., Carver, D.S., Omahony, M.J., and SavilleStones, E.A. (1996). Synthesis of inhibitors of imidazole glycerol phosphate dehydratase. Biorg. Med. Chem. Lett. *6*, 547–552.

Matthews, B.W. (1968). Solvent content of protein crystals. J. Mol. Biol. *33*, 491–497.

Moore, J.A., Parker, A.R., Davisson, V.J., and Schwab, J.M. (1993). Stereochemical course of the *Escherichia coli* imidazole glycerol phosphate dehydratase reaction. J. Am. Chem. Soc. *115*, 3338–3339.

Murshudov, G.N., Vagin, A.A., and Dodson, E.J. (1997). Refinement of macromolecular structures by the maximum likelihood method. Acta Crystallogr. D Biol. Crystallogr. *53*, 240–255.

Navaza, J. (1994). AMORE: an automated package for molecular replacement. Acta Crystallogr. A *50*, 157–163.

Otwinowski, Z., and Minor, W. (1997). Processing of X-ray diffraction data collected in oscillation mode. Methods Enzymol. *276*, 307–326.

Parker, A.R., Moore, J.A., Schwab, J.M., and Davisson, V.J. (1995). *Escherichia coli* imidazole glycerol phosphate dehydratase – spectroscopic characterization of the enzymatic product and the steric course of the reaction. J. Am. Chem. Soc. *117*, 10605–10613.

Petersen, J., Hawkes, T.R., and Lowe, D.J. (1997). The metal-binding site of imidazole glycerol phosphate dehydratase; EPR and ENDOR studies of the oxo-vanadyl enzyme. J. Bioinorg. Chem. *2*, 308–319.

Petersen, J., Hawkes, T.R., and Lowe, D.J. (2000). Oxo-vanadium as a spin probe for the investigation of the metal coordination environment of imidazole glycerol phosphate dehydratase. J. Inorg. Biochem. *80*, 161–168.

Preston, C., and Powles, S.B. (2002). Mechanisms of multiple herbicide resistance in *Lolium rigidum*. ACS Symp. Ser. *808*, 150–160.

Roussel, A., and Cambillau, C. (1991). Silicon Graphics Geometry Partners Directory 86 (Mountain View, CA: Silicon Graphics).

Sinha, S.C., Chaudhuri, B.N., Burgner, J.W., Yakovleva, G., Davisson, V.J., and Smith, J.L. (2004). Crystal structure of imidazole glycerol phosphate dehydratase. J. Biol. Chem. *279*, 15491–15498.

Tada, S., Hatano, M., Nakayama, Y., Volrath, S., Guyer, D., Ward, E., and Ohta, D. (1995). Insect cell expression of recombinant imidazoleglycerolphosphate dehydratase from arabidopsis and wheat and inhibition from triazole herbicides. Plant Physiol. *109*, 153–159.

Tainer, J.A., Getzoff, E.D., Beem, K.M., Richardson, J.S., and Richardson, D.C. (1982). Determination and analysis of the 2 Å structure of copper, zinc superoxide dismutase. J. Mol. Biol. *160*, 181–217.

Whitman, C.P., Aird, B.A., Gillespie, W.R., and Stolowich, N.J. (1991). Chemical and enzymatic ketonization of a 2-hydroxymuconate, a conjugated enol. J. Am. Chem. Soc. *113*, 3154–3162.

Wilkinson, K.W., Baker, P.J., Rice, D.W., Rodgers, H.F., Stillman, T.J., Hawkes, T.R., Thomas, P., and Edwards, L. (1995). Crystallization and analysis of the subunit assembly and quaternary structure of imidazoleglycerol phosphate dehydratase from *Sacchromyces cerevisiae*. Acta Crystallog. D Biol. Crystallgr. *51*, 845–847.

Accession Numbers

The atomic coordinates of *A. thaliana* IGPD have been deposited in the RCSB Protein Data Bank with the accession number 2F1D.